Article:

Assimilable organic carbon cycling within drinking water distribution systems

Frances C. Pick*, Katherine E. Fish, Joby B. Boxall

Sheffield Water Center, Department of Civil and Structural Engineering, The University of Sheffield, Sheffield, United Kingdom

A B S T R A C T

A new conceptual model to describe and understand the role of assimilable organic carbon (AOC) within drinking water distribution systems is proposed. The impact of AOC on both drinking water biofilm and water quality was studied using bespoke pipe loop experimental facilities installed at three carefully selected operational water treatment works. Integrated physical, chemical and biological monitoring was undertaken that highlights the central role of biofilms in AOC cycling, forming the basis of the new conceptual model. Biofilms formed under high AOC conditions were found to pose the highest discoloration response, generating a turbidity (4.3 NTU) and iron (241.5 µg/l) response sufficient to have caused regulatory failures from only 20 m of pipe in only 12 months of operation. This new knowledge of the role of biofilms in AOC cycling, and ultimately impacts on water quality, can be used to inform management and help ensure the supply of high-quality, biostable drinking water.

1. Introduction

The supply of microbially safe, high quality drinking water is one of the most fundamental requirements and functions of every water utility. In order to achieve this, it is often said that the water in drinking water distribution systems (DWDS) should be 'biologically stable'. Although the exact definition is often unclear, biological stability is generally regarded as qualities that minimise the deterioration of water quality between the treatment works and the customers tap. Assimilable organic carbon (AOC), a measure of the labile fraction of dissolved organic carbon, is often suggested as part of biostability assessment, but values are disputed and the roles and cycling of AOC within DWDS are little understood.

2. Background

The term regrowth has been used to describe the recovery of disinfectant-injured cells, whereas aftergrowth has been used to describe microbial growth in a distribution system (Characklis, 1988; van der Kooij, 2003). In this study, (re)growth includes both the recovery of disinfection damaged cells which have passed through the treatment works and the multiplication of organisms within the DWDS itself. AOC is easily utilised by heterotrophic bacteria for growth and is a significant contributor to

biological instability within DWDS (Nescerecka et al., 2014). Globally, AOC is not routinely monitored within operational networks. Low concentrations of AOC have been demonstrated to limit microbial growth, and therefore constitute biostable water, at concentrations spanning ≤10 – 100 µg C/L in DWDS field studies (Van der Kooij, 1992; LeChevallier et al., 1996) and ≤10 – 110 µg C/L within laboratory studies (Ohkouchi et al., 2013; Wang et al., 2014; LeChevallier et al., 2015). However, there is no global consensus as to the AOC concentration that constitutes biostable water. The AOC concentrations representing biostabiltiy within drinking water (≤10 – 100 µg C/L) are thought to differ due to the presence/absence of a disinfection residual, the specific disinfection agent used and other (a)biotic parameters in the DWDS, such as hydraulic retention time, pipe material, DWDS infrastructure (presence of service reservoirs) and temperature. It is therefore critical to consider interactions between AOC and a disinfectant residual when assessing drinking water biostability.

Although AOC has been demonstrated to contribute towards microbial (re)growth within DWDS, the majority of these studies have analysed the effects of AOC on heterotrophic bacteria (Escobar et al., 2001; Van der Kooij 1992) and/or coliforms within the bulk water, and not microorganisms within biofilms. Biofilms within DWDS can generate a decline in water quality, disinfection residual and pipe infrastructure condition, and generate a discolouration response when they mobilise and release materials, such as inorganics, into the bulk water. The biofilm formation rate in drinking water has been shown to be sensitive to changes in

---

* Corresponding author.
  E-mail address: f.pick@sheffield.ac.uk (F.C. Pick).

Table 1

Source water quality, treatment stages and disinfectant types supplying the three full-scale experimental pipe loops.

AOC Concentration[*]	Source Water	Treatment Type	Disinfectant Type	Pipe Loop ID
High ($>$300 µg C/L)	Surface (Reservoir)	RGF	Cl_2	A
Medium ($<$245 µg C/L)	Surface (River)	Membrane	NH_2Cl	B
Low ($<$73 µg C/L)	Groundwater		NH_2Cl	C

AOC: assimilable organic carbon, ID: identification letter, RGF: rapid gravity filter, Cl_2: chlorine, and NH_2Cl: Monochloramine.

[*] The AOC values were determined using the average AOC concentration in the bulk water at each site over the 12 month study period.

AOC concentration within laboratory based studies that typically use biofilm annual reactors (Van der Kooij et al. 1995; Sharp et al., 2001; Okabe et al., 2002). Whilst lab based experimental set-ups go some way to understand the impact of AOC on biofilms within drinking water, bench scale reactors do not accurately reflect the surface to volume ratio, boundary later effect, shear stress and other environmental conditions impacting microorganisms within full scale systems. This study will therefore analyse the relationship between AOC and biofilm formation within fully operational drinking water supply systems.

The mobilisation of microorganisms and associated particles from biofilms can cause discolouration events (Husband and Boxall, 2010) and/or microbial regulatory failures depending on the amount and composition of the detached material. In this study, discolouration is assessed using turbidity, which is a measurement of water clarity obtained by determining the degree of light scattering due to suspended material. Biofilm mobilisation is either generated through daily background release or larger mobilisation events occurring after a change in environmental conditions, such as an increase in the hydraulic shear stress. It is not known how the AOC concentration within post-treated water impacts the discoloration response posed by biofilms if they should become mobilised. The behaviour of particulates within the DWDS has been highlighted as being analogous to biofilm behaviour, with the strength of the layers being dictated by the shear stress imposed on the pipe wall. Data generated in Sharpe et al. (2017) confirmed a positive linear relationship between shear stress and turbidity. The same trend is anticipated here.

3. Material and methods

This research aims to provide an understanding of the relationship between AOC concentration, biofilms and drinking water stability by considering the planktonic and attached microbiology and integrating this with physical and chemical analysis. By studying the effect of different AOC concentrations in the bulk water on biofilm growth, and the subsequent response of biofilms to elevated shear stress (flushing), we seek to determine the role of biofilms in AOC cycling and the resulting impacts on bulk water quality.

3.1. DWDS pipe loop experimental facilities

To explore the impact of AOC on DWDS biofilms and the interaction with bulk water quality, whilst maintaining representative in-pipe conditions (i.e. surface to volume ratios, boundary layer exchange and shear stress mechanisms), biofilms were developed in three purpose-built, full-scale pipe loop experimental facilities (A, B and C) for one year. The pipe loop experimental facilities (Fig. 1) were installed in the field at the exit of three water treatment works (WTW), each being fed with post-treated water supplied directly from the works and containing distinct AOC concentrations. The three sites were classified as either high AOC ($>$300 µg C/L),

medium AOC ($<$245 µg C/L) or low AOC ($<$73 µg C/L) (Table 1). Each system replicated the hydraulic retention time, water chemistry and microbiology of operational DWDS, whilst enabling laboratory level control of bulk water and biofilm sampling. Following the 12 month biofilm growth period, the pipe loops were flushed to provide insight into the effect of AOC concentration on biofilm mobilisation into the bulk water and its impact on various water quality parameters.

Each pipe loop had a different source water (Pipe Loops A & B: surface water, Pipe Loop C: groundwater) and disinfection residual type (Pipe Loop A: chlorine; Pipe Loops B & C: chloramine) (Table 1).Raw water quality data is provided in Supplementary Table 1. While this difference in disinfection residual moves away from pure experimental design with a single parameter changed, this is an unrealistic ambition using operational water treatment works. Furthermore, although there were observed differences between sites, there were also similarities between pipe loops to enable a two-way comparison of environmental and operational factors.

The three experimental pipe loop facilities were purpose built for this study, based on the successful design used by Fish et al. (2017) and Douterelo et al. (2018). The DWDS experimental loops installed at each of the three sites met the same exact design specifications (Fig. 1). Each pipe loop consisted of a 10 m long length of high-density polyethylene (HDPE) PE100 pipe with a 79.3 mm internal diameter. HDPE was selected as it is frequently used in modern DWDS (Fish et al., 2020; Husband et al., 2008). Drinking water was re-circulated around the systems from an enclosed, 30 L (0.03 m^3) tank, via a variable speed pump. An independent system residence time of 24 h was set using a trickle-feed and drain to provide representative water quality of each DWDS, and preserve a baseline nutrient supply and disinfection residual, amongst other water quality parameters.

During the 12 month growth phase, the pipe loop was run at conditioning flow rate of 0.4 l/s (calculated shear stress 0.03 Nm^{-2}, assuming pipe roughness coefficient of 0.075 mm). This flow rate was selected as this was the average flow rate in 75–100 mm diameter pipes within UK DWDS (Husband et al., 2008), and has been used previously in full-scale laboratory tests to develop drinking water biofilms (Douterelo et al., 2014; Fish et al., 2017). The system flow rate was monitored using a Siemens Sitrans F M Mag 6000 flow meter, with flow being controlled by adjusting the control valve at the end of each loop and/or the pump speed. The partially closed final control valve ensured a system pressure of 1.8 bar (18 m) was achieved in the pipe loops. This and a continual upward gradient ensured pipe full conditions were maintained.

Four straight sections (~1 m long) were included in each loop containing 12 apertures (positioned 75 mm apart) into which removable Pennine Water Group (PWG) coupons (Deines et al., 2010) were inserted (Fig. 1) to provide a removable surface for biofilm sampling. The coupons consisted of an outer curved coupon and a removable flat 'insert', which enabled dual analysis of the same
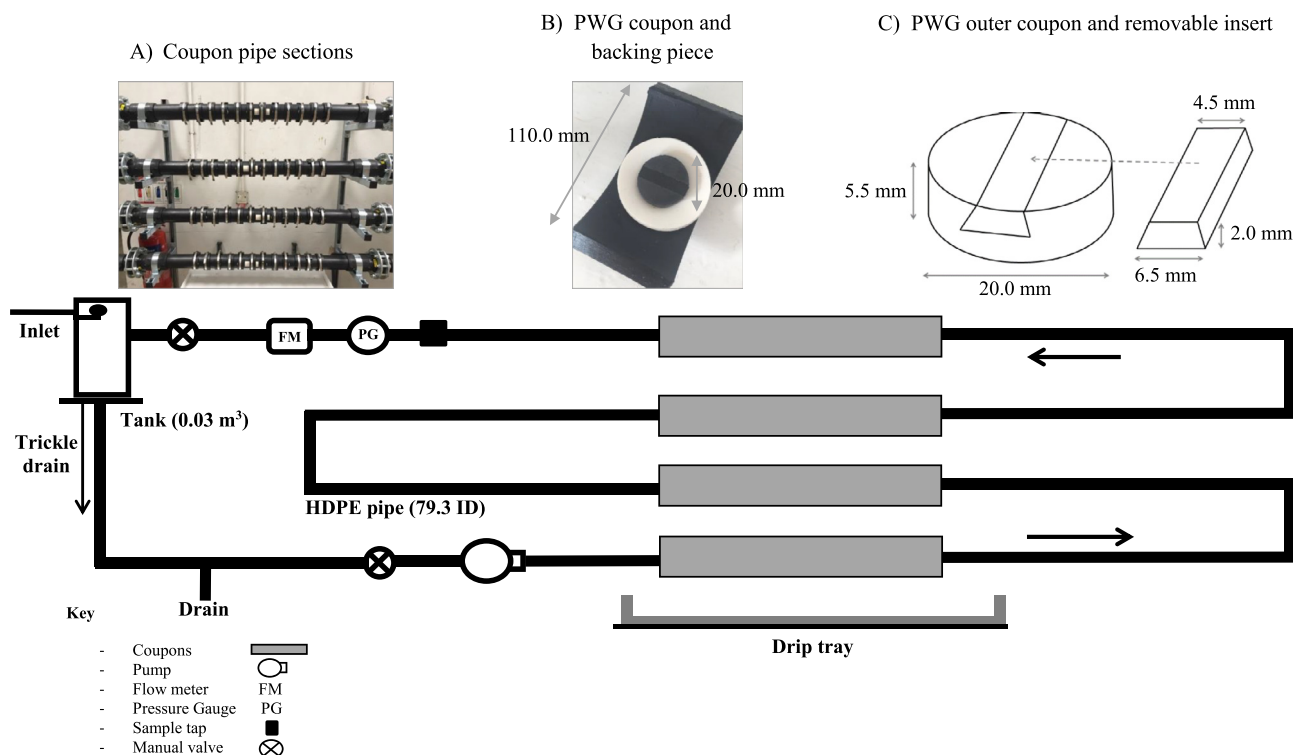
Fig. 1. Pipe loop experimental facility. Each pipe loop (n=3) contained 4 straight coupons sections, with each section containing 12 HDPE PWG coupons (48 in total). A) Coupons inserted into the pipe were secured with brackets. The coupons were positioned at least 10x internal diameter (ID) away from a pipe bend to minimise effects of turbulence generated by the pipe bends; B) HDPE PWG coupon, rubber seal and HDPE backing piece; C) Coupon schematic consisting of a curved outer coupon section and flat insert piece. Any drips leaking from the coupons was captured by the drip tray, and combined and measured with the trickle drain flow to accurately set the system residence time. PWG: Pennine Water Group, HDPE: high-density polyethylene.

sample (Fig. 1, Component C). The curvature of the coupon corresponds to that of the pipe to reduce distortion of boundary layer conditions such as turbulence and shear stress regime. The insert piece had a flat surface designed for microscopy analyses (Deines et al., 2010).

3.2. Growth phase

During the growth phase, biofilms were developed naturally (no inoculum) within each pipe loop facility for one year. Each loop was supplied with treated water at Sites A, B and C respectively, and thus biofilm was grown under high, medium of low AOC conditions. To monitor flow remotely when not on site, three Wi-Fi enabled monitors were designed at The University of Sheffield and installed at each of the three pipe loop sites. The monitors used Arduino technology to monitor and transmit flow data.

3.2.1. Disinfection of pipe loop facilities
Prior to beginning the year-long growth phase, each of the three pipe loops was disinfected for 24 h with a 20 mg/L concentration of a sodium hypochlorite solution (VWR International Ltd, UK) (11–14% free chlorine), which was re-circulated within the system at a maximum flow rate of 5.0 L/s. Each pipe loop was then flushed repeatedly at the maximum flow rate with post-treated water from each WTW until the chlorine concentration decreased to that of the inlet water. Before use, the PWG coupons were sterilised via sonication with a 2% (w/v) sodium dodecyl sulfate (SDS) solution (Fish, 2013).

3.2.2. Water quality sampling
The quality of water circulating in each loop over the 12 months was monitored by collection of discrete bulk water sam-

ples every two weeks ($n = 3$)using sterile 500 mL sample bottles (Aurora Scientific, Bristol, U.K.). Once the distribution line was flushed and the flow reduced, six volumes of 500 mL bulk water were collected from the sample tap marked in Fig. 1.

3.2.3. Biofilm sampling
Coupons for biofilm analysis were collected in triplicate during the growth phase at Day 0, 3 month, 6 month, 9 month and 12 month time periods. Day 0 samples were defined as coupons which were in the pipe loop for ≤ 90 min. The outer coupons (the non-insert component of the coupon) were used to determine the number of intact and damaged cells within the biofilm using flow cytometry. The coupon inserts were used to visually assess biofilm volume using scanning electron microscopy (SEM). These inserts were fixed in 5% formaldehyde solution and stored at 4 °C prior to downstream analysis (Fisher Scientific, UK) (Fish, 2013).

3.3. Flushing phase

3.3.1. Flushing process
Biofilm mobilisation and resulting impact on water quality was assessed by imposing a simulated flushing operation, sequentially increasing the flow rate (1.5, 2.5, 3.5 and 5.0 l/s)and hence boundary shear stress in four steps (0.33, 0.83, 1.55 and 3.02 Nm^{-2}). Flow rate was measured and recorded every 10 s. Due to the relatively short pipe length, head loss was not sufficient for accurate measurement, and hence shear stress was calculated via the Darcy-Wiesbach equation assuming a pipe roughness of 0.075 mm, which is representative of the roughness of PE100 HDPE pipe (Husband et al., 2008). The trickle drain and feed were shut during the flushing phase to ensure accuracy in the assessment of any bulk water quality changes due to the mobilisation of material from the pipe wall.

Table 2
Discrete bulk water parameters ($n = 3$) and online turbidity collected during the growth and flushing phases.

Water Quality Parameter	Instrument/Analysis Method	Range	Resolution	Accuracy
AOC[A]	C6 Flow Cytometer with autosampler (BD Accuri, UK).	10^2–10^7 cells/mL	10,000 events/second. Sample concentration over 5×10^6 cells/mL	–
TCC[B] **and ICC**[C]	C6 Flow Cytometer with autosampler (BD Accuri, UK).	10^2–10^7 cells/mL	10,000 events/second. Sample concentration over 5×10^6 cells/mL	–
TOC[D]	Formacs high temperature catalytic combustion system (Skalar Analytical B.V., Breda, Netherlands).	100 ppb[F]–5000 ppm[G] carbon	–	–
TON[E] **and Phosphate**	Aquakem 600 Discrete analyser (Thermo Fisher Scientific Ltd., Loughborough, U.K).	Spectral range 340–880 nm. Halogen lampabsorbence range 0–0.25 A	Halogen lampabsorbence resolution of 0.001 A	Halogen lampabsorbence reproducibility of SD ≤0.005A at 2 A.
Iron and Manganese	PerkinElmer Nexion 300X ICPMS Spectrometer	–	–	–
Total and Free Chlorine	Pocket colorimeter (Hach-Lange, Salford, U.K.)	0.00 to 5.00 mg/L	0.01 mg/L	± 0.02 mg/L
Turbidity	Hach handheld 2100Q formazine calibrated turbiditymetre	0–1000 NTU[H]	±1% of reading or 0.01 NTU	±2%
Online Turbidity	ATI A15/76 (Analytical Technology Inc, UK)	0.001 NTU - 4000 NTU	0.001 NTU	± 5% of reading or ± 0.02 NTU
Temperature	Sealey THC100 Thermometer	−50 °C to +70 °C	–	±1 °C
pH	ROSS Ultra pH electrode (Thermo Fisher Scientific Ltd., Loughborough, U.K.)	0–14	–	± 0.01
Flow	Siemens Sitrans fm mag 6000 flowmetre	–	–	± 0.2% of the flow rate

[A] Assimilable Organic Carbon;.
[B] Total Cell Count;.
[C] Intact Cell Count;.
[D] Total Organic Carbon;.
[E] Total Organic Nitrogen;.
[F] parts per billion;.
[G] parts per million;.
[H] Nephelometric Turbidity Units.

3.3.2. Water quality

Discrete samples ($n = 3$) were collected after five turnovers at each flow rate when all mobilisation had occurred and the mobilised material was well mixed into the bulk water. Discrete samples from the flushing phase were analysed for the bulk water quality parameterslisted in Table 2.Turbidity data was also collected continuously throughout the flushing phase using an ATI monitor (Table 2) connected to a tapping point just upstream of the control valve with a return to the system tank (Figure 1). The turbidity time series showed that stable turbidity levels were achieved within three turnovers, with five turnovers being used to provide additional confidence.

3.3.3. Biofilm sampling

Biofilm samples (coupons) were taken post-flush (after the final flushing step) and collected in triplicate. Coupons were positioned along either side of the pipe length, with the exception of nine top or bottom positioned coupons which were used to determine if the coupon position within the pipe influenced the biofilm. Top and bottom positioned coupons (outer coupons only) were analysed to determine the number of intact and damaged cells within the biofilm using flow cytometry.

3.4. Water quality analysis

3.4.1. Water quality sampling

Bulk water discrete samples from growth and flushing phases were analysed for the water quality parameters displayed in Table 2. In addition, continuous turbidity measurements were conducted using an online ATI (Analytical Technology Inc, UK) turbidity logger.

3.4.2. AOC

AOC was analysed for all bulk water discrete samples from growth and flushing phases using the method developed and proven in Pick et al. (2019). The AOC methodology combined the known strain inoculum approach, with a larger inoculum volume and flow cytometric enumeration to increase the speed and reproducibility of evaluating AOC concentration. In summary, 40 ml water samples were collected into glassware which has been rendered organic carbon free using the method described in Pick et al. (2019). Samples were collected using the method outlined in Section 3.2.2 and dechlorinated using sodium thiosulphate. In the lab samples were pasteurised in a 70 °C water bath for 30 min, before being inoculated with 10,000 CFU/mL of either *Pseudomonas fluorescens* strain P-17 (P-17) or *Spirillum* strain NOX (NOX) into separate vials and incubated at 15°C. Samples were enumerated on days 6, 7 and 8 using the flow cytometry protocol outlined in Section 3.4.3. The averaged cell counts on day 6, 7 and 8 were converted to AOC values using pre-derived yield value of 4.1 × 10^6 CFU P-17/μg acetateC and 1.2 × 10^7 CFU-NOX/μg acetate-C (Van der Kooij et al. 1982). The two known strains, cultures of P-17 (ATCC 49,642) and NOX (ATCC 49,643) were acquired from the American Type Culture Collection (ATCC). The preparation of the stock cultures was performed as described in LeChevallier et al. (1993) and Aggarwal et al. (2015). AOC controls were performed including residual chlorine vials to check the chlorine content after dechlorination, growth controls to determine if samples were limited by nutrients other than carbon, blank controls to check for carbon contamination and yield controls to check the growth yield of the two bacterial strains.

3.4.3. Flow cytometry

Planktonic total (TCC) and intact cell count (ICC)(cells/mL) in the bulk water were measured using the flow cytometry method outlined in Fish et al. (2020). Bulk water samples for flow cytometry analysis were collected (using the sampling method outlined in Section 3.2.2) into bottles pre-treated with sodium thiosulphate

3% (w/v) to dechlorinate the samples before analysis. In summary, 500 μl water samples were stained with 5 μl SYBR Green (Life Sciences, California, USA) for TCC. 500 μl water samples were stained with 6 μl SYBR Green/ Propidium Iodine mixture (Life Sciences, California, USA) (with a final concentration of 1x SYBR Green and 3 μM PI) for ICC. Samples were analysed using BD Accuri C6 Flow Cytometer with autosampler (BD Accuri, UK), with a fixed gate plot as described in Fish et al., 2020. All appropriate negative controls were performed, including negative controls for stains, and calibration beads were run daily.

3.5. Biofilm analysis

3.5.1. Scanning electron microscopy (SEM)

SEM was used to provide a qualitative assessment of biofilm accumulation, giving an indication of differences in surface coverage and the physical structure of the biofilms. One 12 month insert was analysed from each loop, with each biofilm sample being imaged at 1000x and 5000x magnification, with a total of 50 images being taken per sample. All SEM sample preparation and imaging was undertaken at the Biomedical Science Electron Microscopy Unit, The University of Sheffield and analysed as described in Douterelo et al. (2016).

3.5.2. Flow cytometry of biofilm samples

Biofilm suspensions were prepared for flow cytometry using the protocol published in Fish et al. (2020). The outer coupon was placed in a petri dish with 30 ml of sterile phosphate buffer and repeatedly brushed using a sterile toothbrush (Fish, 2013). Negative controls were run on the flow cytometer using phosphate buffer solution stained for TCC and ICC. A 0.5 mL volume of the biofilm suspension was stained and analysed in accordance with the bulk water flow cytometry protocol. To convert the cell counts into cell concentrations (ICC/mm^2 or TCC/mm^2), the following equation was used:

$$ICC\ or\ TCC = \frac{(Count/Volume\ analysed)\ x\ Total\ volume\ of\ sample}{SA}$$

Where the count is the total or intact cell count, volume analysed is the volume of sample that was processed in the flow cytometer (50 μl), the total volume of samples in this case was 30 ml (30,000 μl) and SA is the surface area from which the biofilm was removed. All the raw biofilm data were converted into ICC mm^2 or TCC mm^2. Preliminary experiments of technical replication showed no difference so only biological replicates were undertaken ($n = 3$).

3.6. Data analysis

The normality of the data was analysed using the Shapiro-Wilks test and parametric (ANOVA and Tukey) or non-parametric tests (Kruskal Wallis and two-sample Wilcoxon), as appropriate, to identify any differences in water quality parameters between experiments. Data collected during the flushing phase was plotted against shear stress and a linear model and regression analysis performed to identify relative changes (each loop was analysed separately). The R^2 and p values were used to assess the fit of the linear model to the data and the significance of the gradient, so as to determine which parameters responded significantly to the elevation in shear stress. All statistical analysis and graphical plots were generated in R v3.5.2 (R Foundation for Statistical Computing Platform, 2018) with a significance level of <0.05.

4. Results

4.1. Growth water quality

Results from repeated sampling of the bulk water quality in each of the pipe loops during the 12 month growth period are presented in Table 3. The intended dominant difference between the sites was AOC, with concentrations highest within Pipe Loop A, mid-range in Pipe Loop B and lowest in Pipe Loop C (Table 3). As these are operational sites, other parameters also varied between the sites, as shown in Table 3. TCC and ICC within the bulk water mirrored the AOC trend, being consistently highest in Pipe Loop A throughout the growth period. Total organic nitrogen and phosphate within the bulk water supplying each pipe loop were not statistically different between the three sites (Table 3).

4.2. Biofilm visualisation

SEM images of 12 month biofilm samples in Fig. 2 show that the biofilms which accumulated in each pipe loop exhibited a distinct difference in both quantity and structure of biofilm between sites supplied by bulk water containing different AOC concentrations. The EPS matrix primarily made up of carbohydrates and proteins, helps to form the physical structure of the biofilm.

Visual, qualitative assessment of these images suggests that the biofilm developed on coupons in Pipe Loop A, supplied by water with the highest AOC concentration, had more extensive biofilm coverage, with a more open, sponge like extracellular polymeric substance (EPS) matrix, compared to Pipe Loop B or Pipe Loop C where the EPS is increasingly more closed or compact. Angular inorganic particles were visualised within SEM images of biofilms from all three pipe loops.

4.3. Biofilm cell enumeration

In all cases, both the TCC and the ICC of the biofilm increased during the 12 month growth-phase, and decreased during flushing due to an increase in the shear stress. The greatest increase in both biofilm TCC and ICC throughout the 12 month growth phase was seen in Pipe Loop A; the pipe loop supplied with bulk water containing the highest concentration of AOC. The rate of biofilm growth was different at each site, with the greatest rate occurring in Pipe Loop A and the slowest rate in Pipe Loop C. Biofilm growth within Pipe Loop A appeared to slow after 6 months, perhaps indicating that biofilm growth was starting to tend towards an equilibrium state, whereas biofilm growth within the other two pipe loops was still increasing approximately linearly. Analysis of coupon position within each experimental pipe loop showed no significant difference with respect to the biofilm cell count or the biofilm appearance (as assessed using SEM imaging).

4.4. Flushing response

4.4.1. Biofilm cells

Comparison of the final two points in Fig. 3 show the mobilisation of cellular material from the biofilm phase due to flushing. Following on from flushing, the greatest loss of TCC from the biofilm was experienced within Pipe Loop A (60% decline in TCC), as compared to 28% loss TCC within Pipe Loop B and 23% loss TCC within Pipe Loop C. The greatest loss of ICC occurred within Pipe Loop B (30% loss of ICC) in comparison to a 24% decline within Pipe Loop A and 18% decline within Pipe Loop C.

4.4.2. Aesthetics and inorganics

All three pipe loops exhibited a positive turbidity, iron and manganese response as the shear stress was raised (Fig. 4), indicating the mobilisation of small particles and inorganic material

Table 3

Bulk water quality during the formation of biofilms over a 12 month period at Pipe Loop A, Pipe Loop B and Pipe Loop C.

Water Quality Parameter	Pipe Loop A Mean (SD[A])	Pipe Loop B Mean (SD[A])	Pipe Loop C Mean (SD[A])
AOC (µg C/L)	300 (29)	245 (32)	73 (13)
TCC (cells/mL)	118,668 (133,077)	1691 (3221)	450 (1710)
ICC (cells/mL)	569 (1451)	206 (2125)	49 (45)
Total Chlorine (mg/l)	0.89 (0.11)	1.34 (0.15)	0.64 (0.10)
Free Chlorine (mg/l)	0.80 (0.12)	0.15 (0.05)	0.52 (0.06)
Turbidity (NTU)*	0.2 (0)	0.2 (0)	0.2 (0)
Iron (µg/L)*	<7[B]	<7[B]	<7[B]
Manganese (µg/L)	5.98 (4.09)	4.96 (3.01)	2.05 (0.40)
TOC (mg/L)	1.41 (0.31)	1.49 (0.43)	0.33 (0.15)
Total Organic Nitrogen (mg/L)*	1.22 (0.25)	1.20 (0.31)	1.16 (0.30)
Phosphate (mg/L)*	0.77 (0.12)	0.87 (0.26)	0.84 (0.21)

Replication $n = 3$, samples collected fortnightly for 12 months = 72 samples.

[A] SD = standard deviation;.

[B] Below the limit of detection. AOC = Assimilable Organic Carbon; TCC = Total Cell Count; ICC = Intact Cell Count; NTU = Nephelometric Turbidity Units; TOC = Total Organic Carbon. Parameters marked with * did not statistically differ between sites.

Table 4

Gradient, R^2 and P values for turbidity, iron and manganese in bulk water within pipe loop experimental facilities at Pipe Loop A, Pipe Loop B and Pipe Loop C, during the flushing phase.

Pipe Loop ID	Turbidity			Iron			Manganese		
	Gradient[A]	$R^{2\,B}$	p value[C]	Gradient[A]	$R^{2\,B}$	p value[C]	Gradient[A]	$R^{2\,B}$	p value[C]
A	1.39	0.8902	0.0160	72.58	0.8947	0.0150	11.58	0.9110	0.0116
B	1.13	0.9720	0.0020	54.43	0.9300	0.0080	9.55	0.9447	0.0056
C	0.63	0.9374	0.0068	36.06	0.8948	0.0150	4.30	0.9564	0.0039

[A] The gradient defines the rate of change along the regression line;.

[B] R^2 value indicates the goodness of fit of the linear regression model to the data, nearer to 1 the better the fit;.

[C] A significant p-value (<0.05 significant; >0.05 weak evidence) indicates the significance of the gradient, so as to determine which parameters responded significantly to the elevation in shear stress.

from the pipe wall. Pipe loop A, supplied by bulk water containing the highest AOC concentration, exhibited the greatest turbidity response during flushing, increasing from 0.27 to 4.75 NTU. Pipe Loop A therefore generatedthe greatest discoloration response. Conversely, Pipe Loop C supplied by post-treated ground water containing the lowest AOC concentration experienced the smallest turbidity response increasing from 0.2 to 2.15 NTU. The concentration of iron and manganese in the bulk water during flushing was highest in Pipe Loop A, and lowest in Pipe Loop C. All three sites contained relatively low iron (mean=12.53 µg/L, standard deviation (SD)=1.27 µg/L in Pipe Loop A, mean=10.07 µg/L, SD=1.11 µg/Lin Pipe Loop B and mean=6.83 µg/L, SD=0.57 µg/L in Pipe Loop C) and manganese (mean=8.67 µg/L, SD=0.55 µg/L in Pipe Loop A, mean=5.10 µg/L, SD=0.30 µg/Lin Pipe Loop B and mean=3.10 µg/L, SD=0.20 µg/L in Pipe Loop C) concentration prior to flushing. Pipe loop A exhibited the greatest increase in iron (increase of 225.00 µg/L) and manganese (increase of 33.90 µg/L) due to the simulated flushing.

The trends for increasing turbidity, iron and manganese with increasing boundary shear stress are all linear (Fig. 4). The gradient, R^2 and p values quantifying this for each of the pipe loop experimental facilities are listed in Table 4. Pipe Loop A can be seen to have consistently the highest gradient value, confirming the greatest turbidity, iron and manganese was experienced within Pipe loop A. In contrast, the smallest gradient can consistently be found within Pipe Loop C.

### 4.4.3. Bulk water cellular material

The changes in bulk water cellular material is shown in Fig. 5. It should be noted that initial values are a function of the differences in the bulk water between the sites (as observed throughout the growth phase) (Table 3). Of interest is the change from the initial values. During flushing, all three pipe loops exhibited

an increase of both TCC and ICC (Fig. 5 A& B) within the bulk water. TCC increased by the greatest extent within Pipe Loop A and Pipe Loop B, increasing by 21,229 cells/mL within Pipe Loop A, and 20,595 cells/mL within Pipe Loop B. The bulk water within Pipe Loop C had the smallest increase in TCC during flushing, with the TCC increasing by 6376 cells/mL. Although Pipe Loop A contained the highest TCC within the bulk water at the end of and during the growth phase, proportionally the change in TCC during flushing was greatest in Pipe Loop C, having 25 times more cells in the bulk water by the end of flushing compared to the start. In comparison, Pipe Loop B exhibited an 11 fold increase in cells within the bulk water, and Pipe Loop A, only a two fold increase in cell mobilised into the bulk water.

The greatest increase in ICC during flushing occurred within Pipe Loop A (increase of 16,972 cells/mL), followed by Pipe Loop B (increase of 10,687 cells/mL) and finally the smallest increase in ICC within Pipe Loop C (4816 cells/mL). However, as with TCC, the change in ICC relative to initial value was greatest in Pipe Loop C, increasing by67 times, with 20 times increase in Pipe Loop B and 12 times increase in Pipe Loop A. This also reveals that the greatest proportion of cells being mobilised from the pipe wall were intact and not damaged/dead.

As with turbidity and inorganic parameters, the mobilisation of intact and damaged cells due to the increases in shear stress was visually linear in most cases (Fig. 5 and Table 5). Despite the largest turbidity, iron, manganese and ICC response being observed in Pipe Loop A, the largest TCC gradient was found in Pipe Loop B.

The response of TOC and AOC mobilisation into the bulk water during the flushing phase of Pipe Loops A, B and C is plotted in Fig. 6. The behaviour of TOC mirrored all other aforementioned water quality parameters (turbidity, iron, manganese, TCC and ICC); TOC concentration was consistently highest within Pipe Loop A throughout the flushing phase and lowest in Pipe Loop C.
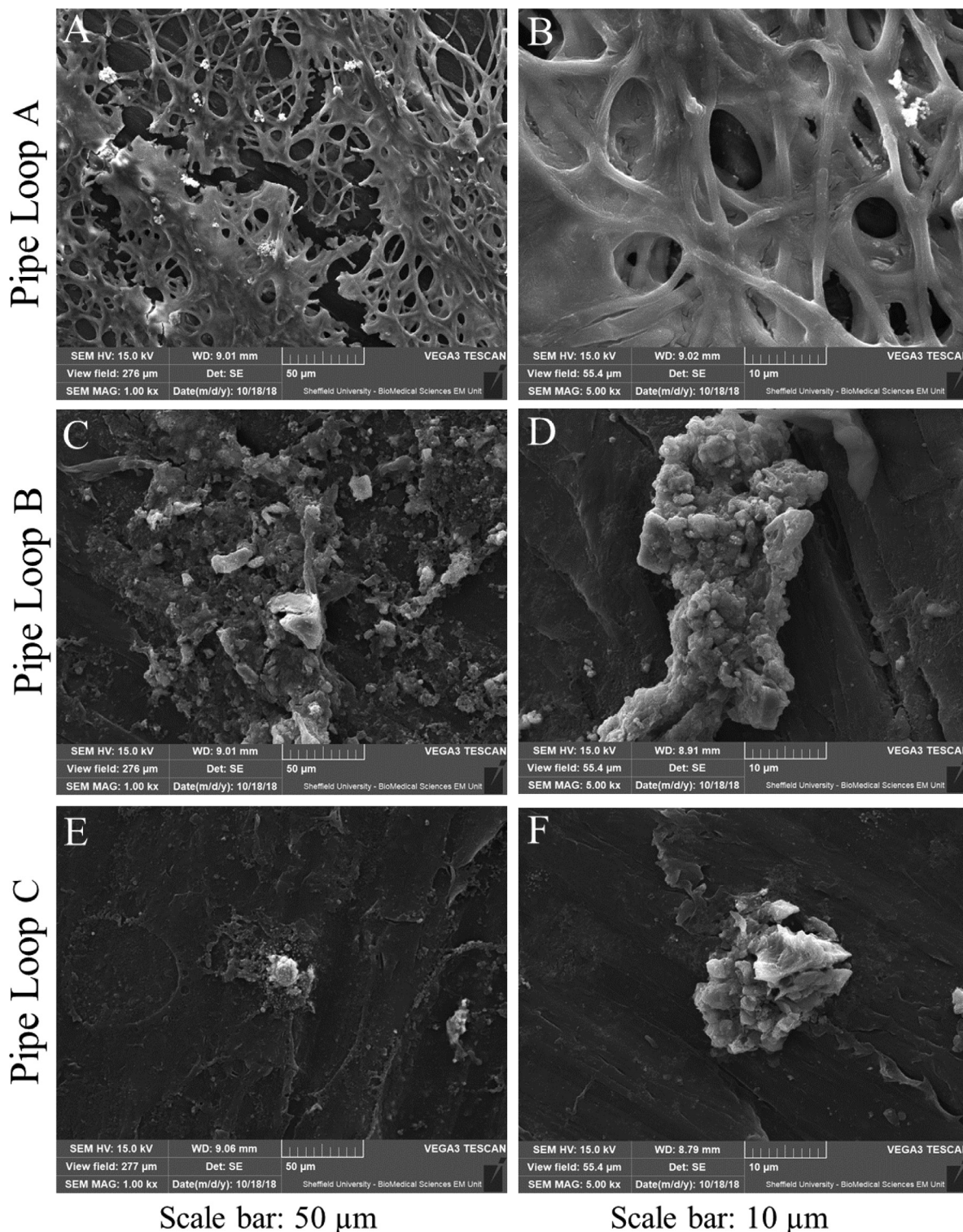
Fig. 2. Representative SEM images of 12 month biofilm samples from Pipe loop A (A-B), Pipe loop B (C-D) and Pipe loop C (E-F), imaged at the magnification indicated by the scale bar on each image. Scale bar of images on left = 50 µm, scale bar of images on right = 10 µm.

The greatest increase in TOC within the bulk water was experienced within Pipe Loop A (increase of 9.50 mg/L), followed by Pipe Loop B (increase of 6.53 mg/L) and finally Pipe Loop C (4.53 mg/L).

4.4.4. Organic carbon

All bulk water samples collected during flushing, including turbidity, iron, manganese, TCC, ICC and TOC exhibited a clear site ef-

fect. The largest response in each of these parameters during flushing was consistently observed within Pipe Loop A (characterised by a high AOC concentration), with the smallest response being observed within Pipe Loop C (characterised by a high low concentration).The AOC (ANCOVA on raw data: $F \geq 185$, $p \leq 0.001$) and TOC (ANCOVA on raw data: $F \geq 13$, $p = 0.002$) responses during flushing were found to be statistically different between sites.
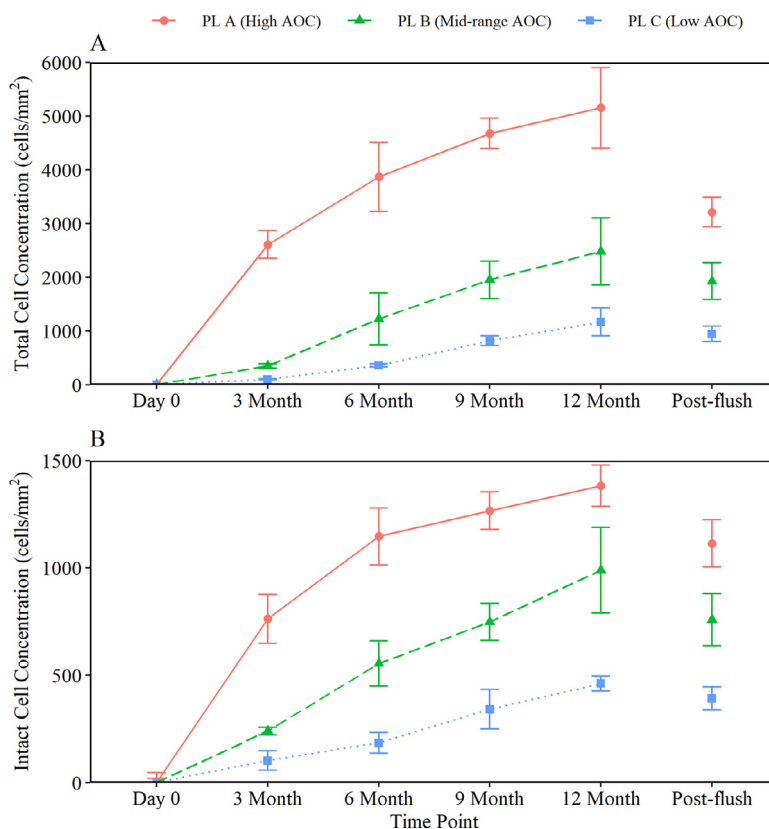
Fig. 3. A) Total cell count (TCC) and B) Intact Cell Count (ICC) within drinking water biofilms within pipe loop experimental facilities at Pipe loop A, Pipe loop B and Pipe loop C, during the growth (Day 0 −12 month) and flushing (post-flush) phase. Average ($n = 3$) ±SStDev plotted, lines are plotting the average value. PL = pipe loop. During the growth phase there were significant difference in both biofilm TCC ($p = 0.002$) and biofilm ICC ($p<0.001$) between the three pipe loops.

Table 5
Gradient (G), R^2 and P values for total cell count (TCC) and intact cell count (ICC) in bulk water within pipe loop experimental facilities at Pipe Loop A, Pipe Loop B and Pipe Loop C, during the flushing phase.

Pipe Loop ID	TCC			ICC		
	Gradient[A]	R^{2B}	p value[C]	Gradient[A]	R^{2B}	p value[C]
A	5902	0.8029	0.0396	5100	0.7362	0.0629
B	6870	0.9514	0.0046	3394	0.9621	0.0032
C	2072	0.9982	0.0000	1551	0.8656	0.0218

[A] The gradient defines the rate of change along the regression line;.
[B] R^2 value indicates the goodness of fit of the linear regression model to the data, nearer to 1 the better the fit;.
[C] A significant p value indicates that the gradient is significantly different from 0.

Table 6
Gradient (G), R^2 and p values for total organic carbon (TOC) and assimilable organic carbon (AOC) in bulk water within pipe loop experimentalfacilities at Pipe Loop A, Pipe Loop B and Pipe Loop C, during the flushing phase.

| Pipe Loop ID	TOC			AOC		
	Gradient[A]	R^{2B}	p value[C]	Gradient[A]	R^{2B}	p value[C]
A	3.01	0.9500	0.0048	28	0.5840	0.1325
B	2.20	0.9030	0.0132	40	0.9969	0.0001
C	1.31	0.7857	0.0452	36	0.8830	0.0176

[A] The gradient defines the rate of change along the regression line;.
[B] R^2 value indicates the goodness of fit of the linear regression model to the data, nearer to 1 the better the fit;.
[C] A significant p value indicates that the gradient is significantly different from 0.

Despite this, in comparison to other drinking water parameters, the amount of AOC mobilised from the biofilm was surprisingly similar, independent of the background AOC concentration during growth (Fig. 6B). As with cell counts, the concentration of AOC at the end of the growth phase/start of flushing were different across the three pipe loops, with flushing starting from values consistent with those in Table 3.However, the increase in AOC concentration from pre- to post-flush was unexpectedly similar between sites, with a 115 µg C/L increase in AOC within Pipe Loop A, 120 µg C/L increase in AOC within Pipe Loop B, and a 115 µg C/L increase in AOC within Pipe Loop C.

Linear trends in the mobilisation of TOC and AOC as a function of increasing shear stress were observed (Fig. 6). Despite the largest TOC gradient being experienced within Pipe Loop A, the smallest AOC gradient was also experienced within Pipe Loop A (Table 6). The R^2 value for AOC concentration within Pipe Loop A was considerably lower than other pipe loops, suggest-

ing the AOC response during flushing within Pipe Loop A was non-linear.

5. Discussion

5.1. The impact of AOC on plank tonic growth and biofilm accumulation

This study presents the first investigation of the interactions between AOC concentration and biofilms within an operational DWDS environment. The findings herein demonstrate that AOC influences the appearance (Fig. 2) and cell count (Fig. 3) of biofilms residing at the pipe wall. This study found that the greatest growth of cells in the biofilm occurred when the AOC concentration within the bulk water was >300 µg C/L, as demonstrated in Pipe Loop A. Similar to the trends identified in the AOC data, TCC and ICC within the bulk water were also found to be highest in Pipe Loop
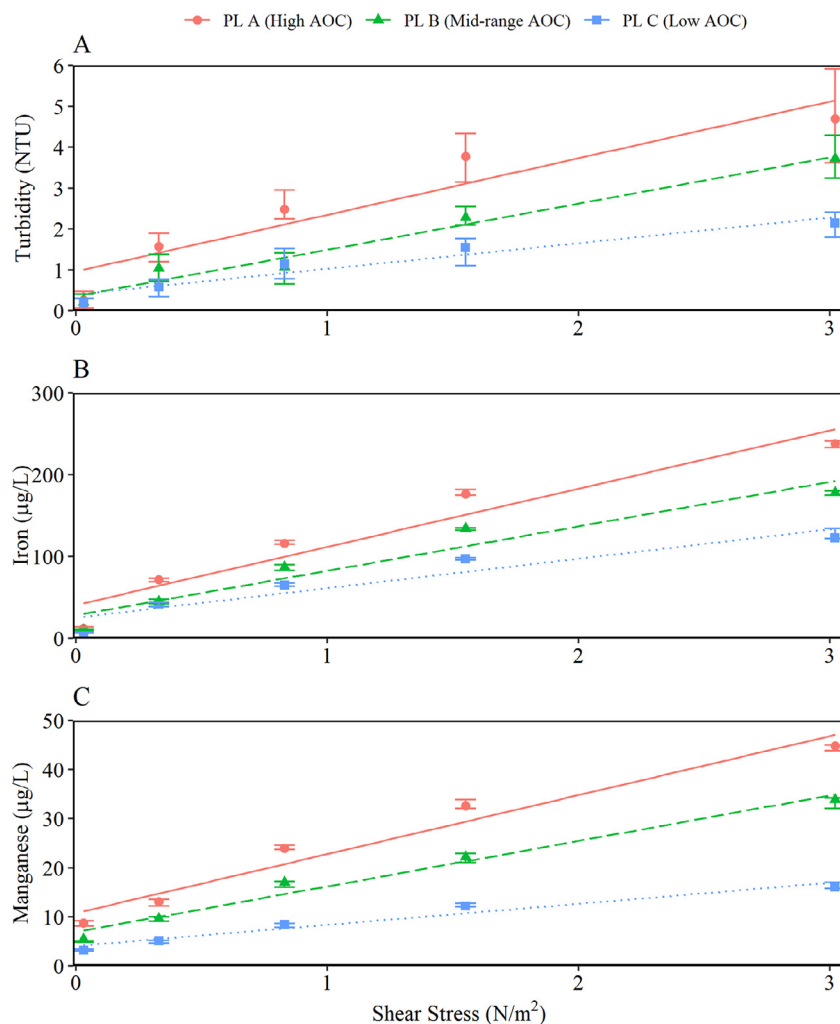
Fig. 4. A) Turbidity B) Iron ($n = 3$) C) Manganese ($n = 3$) in bulk water within pipe loop experimental facilities at Pipe loop A, Pipe loop B and Pipe loop C, during flushing. Averages from the 5th turn over of the continuous turbidity data are presented $\pm$ StDev.Lines illustrate the linear model used to determine which parameters responded significantly to the elevation in shear stress. R^2 and gradient values are provided in Table 4.PL = pipe loop.AOC concentration regimes differed in their turbidity (ANCOVA on raw data: $F \geq 15$, $p = 0.001$), iron (ANCOVA on raw data: $F \geq 7$, $p = 0.014$) and manganese (ANCOVA on raw data: $F \geq 24$, $p \leq 0.001$) responses during flushing.

A during the growth period. This correlation could be due to higher AOC concentrations supporting planktonic (re)growth, which indirectly seeds the biofilm and increases initial biofilm colonisation. However, as identified in Supplementary Figures 1, 2 and 3, bulk water TCC and ICC exhibited periodic spikes over short spaces of time, indicating that TCC and ICC were likely impacted by upstream events in the operational systems and therefore not consistently different between sites. AOC was found to be more consistently different between sites and is therefore more likely to have been the key parameter shaping biofilm development.

Biofilms affect water quality by the processes they mediate during growth (bio-corrosion), and from ongoing exchange and mobilisation into the bulk water.Pick et al. (2019) found that, during DWDS network sampling, pipe dominated areas of the network exhibited a net decrease in the AOC concentration, suggesting that AOC in the bulk water was being used to support microbial growth within the biofilm attached to the pipe wall. Crucially, the AOC concentration in drinking water is impacted by interactions occurring in the bulk water, and also those taking place in biofilms.

The increase in TCC and ICC within the biofilm formed under the highest AOC concentration studied, slowed between Month 9 and Month 12, suggesting that biofilms will mature faster at high

AOC concentrations. The rate of biofilm maturation is dependant on a host of factors including nutrient availability, hydrodynamics, rate of oxygen perfusion (Dunne, 2002). This study found that even in Pipe Loop C where the AOC concentration was low, although microbial regrowth within the biofilm was limited, it did still occur. Pipe Loop C had the lowest concentration of AOC (<73 µg C/L), meaning it would be classed as biologically stable based on values cited in the literature ($\leq 10 - 110$ µg C/L) (Van der Kooij, 1992; LeChevallier et al., 1996; Ohkouchi et al., 2013; Wang et al., 2014; LeChevallier et al., 2015).Similarly,Okabe et al. (2004)found that biofilms still formed on pipe surfaces (within a laboratory experiment)which were exposed to drinking water containing an AOC concentration of 39 µg C/L. Even when nutrient levels are extremely low within DWDS, non-oligotrophs are able to survive in this environment by residing within biofilms where nutrients are elevated (Volk and LeChevallier, 1999). Thus, while biological stability is dependant on AOC concentration, there is no universal AOC threshold for biological stability due to the interaction and influence of both planktonic and biofilm processes.

While AOC was intended as the dominant factor that differed between the sites studied here, the disinfection residual was also different. Pipe Loop A was supplied by chlorinated water, whereas
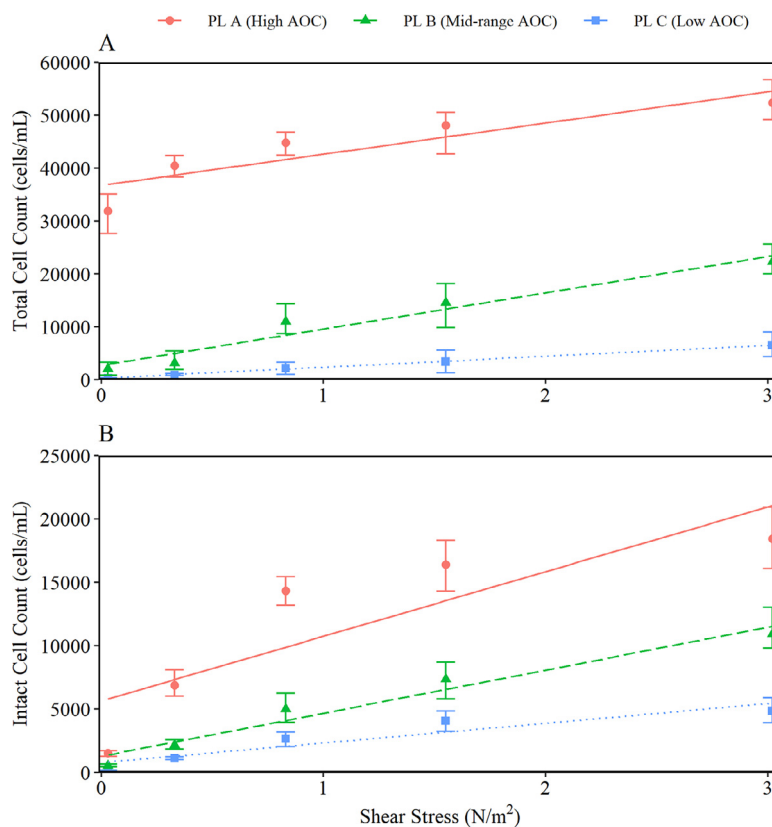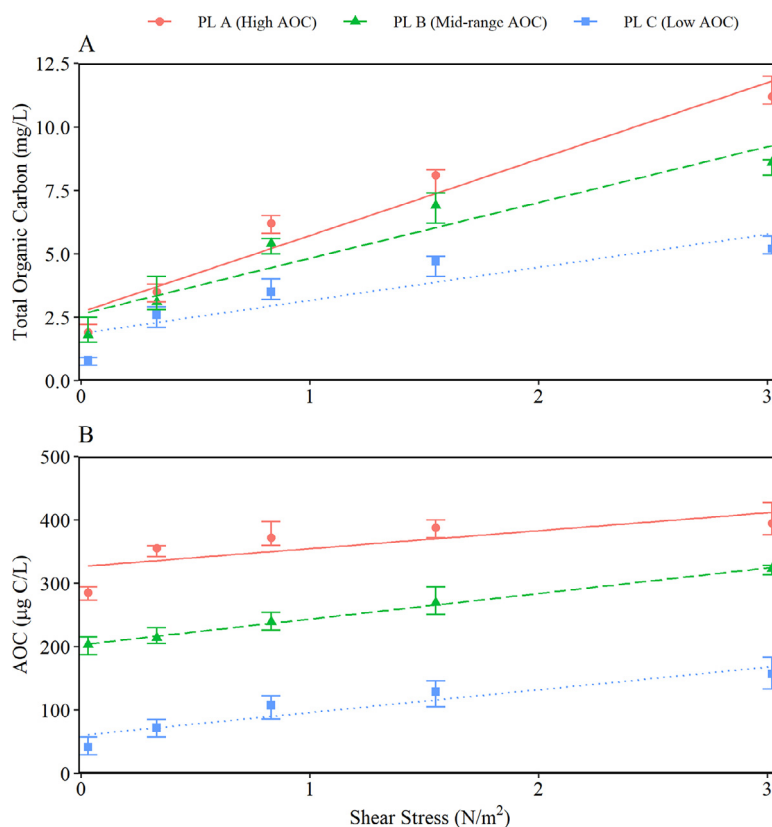
Fig. 5. A) Total cell count (TCC) ($n = 3$) B) Intact Cell Count (ICC) ($n = 3$) in bulk water within pipe loop experimental facilities at Pipe Loop A, Pipe Loop Band Pipe Loop C, during the flushing phase. Lines illustrate the linear model used to determine which parameters responded significantly to the elevation in shear stress. R^2 and gradient values are provided in Table 5. PL = pipe loop. AOC concentration regimes differed in their TCC (ANCOVA on raw data: $F \geq 357$, $p<0.001$) and ICC (ANCOVA on raw data: $F \geq 17$, $p< 0.001$) responses during flushing.

Pipe Loop B and Pipe Loop C were supplied with chloraminated water. In this study, the use of chlorine correlated with the highest bulk water TCC and ICC load, the highest AOC concentration and the greatest biofilm growth. When comparing biofilm growth within the two sites with a monochloramine residual, the greatest biofilm growth occurred in Pipe Loop B despite it having double the total chlorine concentration of Pipe Loop C (Table 3). This demonstrates that AOC has a greater effect than chlorine concentration on biofilm growth. Although the application of a disinfection residual is able to limit planktonic cell growth within DWDS (Gillespie et al., 2014), chlorine can oxidise the natural organic matter in drinking water to produce AOC that can support the growth of heterotrophic bacteria (Liu et al., 2002; Ramseier et al., 2011). This highlights the need for water utilities to prioritise AOC reduction at the WTW, rather than reliance on increasing disinfection residual within the DWDS.

The AOC concentration was found to impact biofilm coverage and appearance, as identified via SEM imaging (Fig. 2). Biofilms formed under elevated AOC concentrations had a thicker, spongier appearance, supporting the theory that biofilm architecture is determined by environmental conditions, such as carbon availability (Karthikeyan et al., 2001). Microscopy-based studies have indicated that carbon concentration can affect biofilm physical structure with a carbon increase altering a thin, open biofilm to a thicker structure supporting mushroom cell clusters (Stoodley et al., 2001). Biofilm physical structure can also facilitate the mass transfer of nutrients to microorganisms residing within the biofilm via water channels (de Beer and Stoodley, 1995; de Beer et al. 1996). Whilst the impact of AOC concentration on EPS production has yet to be explored, the results presented here suggest that AOC concentration has an impact on biofilm physical structure.

5.2. The impact of AOC on biofilm mobilsation and bulk water quality

Turbidity, inorganic and cell count data all exhibited a linear increase in the bulk water due to increasing shear stress. This observation shows that all biofilm and other material accumulated within the different pipe loops had material adhered with a range of strengths from the weakest to the most strongly adhered. Although these commonalities were observed, the discoloration response varied between the three sites, with a low AOC concentration (<73 μg C/L) in the bulk water resulting in the lowest discoloration response, and a high concentration of AOC (defined as >300 μg C/L) in the bulk water resulting in the largest discoloration response (Fig. 4). This study found that when bulk water AOC concentration is high, sufficient iron can accumulate over the course of a year to generate an iron failure (over 200 μg/l DWI, 2017) when flushing. This therefore supports previous findings that biofilms are key drivers of discolouration within DWDS (Husband et al., 2016), and that this process is exasperated by an increased bulk water AOC concentration. With increasing AOC concentration, there was more material available within the biofilm, which could then become mobilised during small-scale, daily mobilisation, or during event induced mobilsation (when the internal strength of the biofilm was exceeded by external shear forces). Picioreanu et al. (2001) used 2D mathematical modelling and found that increased biofilm growth rate correlated with small scale, regular release events, possibly because microorganisms preferentially used energy in cell replication rather than EPS production. The biofilms exposed to bulk water containing a higher concentration of AOC in this study (Pipe Loop A) had a higher growth rate than those in Pipe Loop B or C, forming more EPS and incorporating greater amounts

Fig. 6. Total organic carbon (TOC) ($n = 3$) and assimilable organic carbon (AOC) ($n = 3$) in bulk water within pipe loop experimentalfacilities at Pipe Loop A, Pipe Loop B and Pipe Loop C during the flushing phase.Lines illustrate the linear model used to determine which parameters responded significantly to the elevation in shear stress. R^2 and gradient values are provided in Table 6. PL = pipe loop.
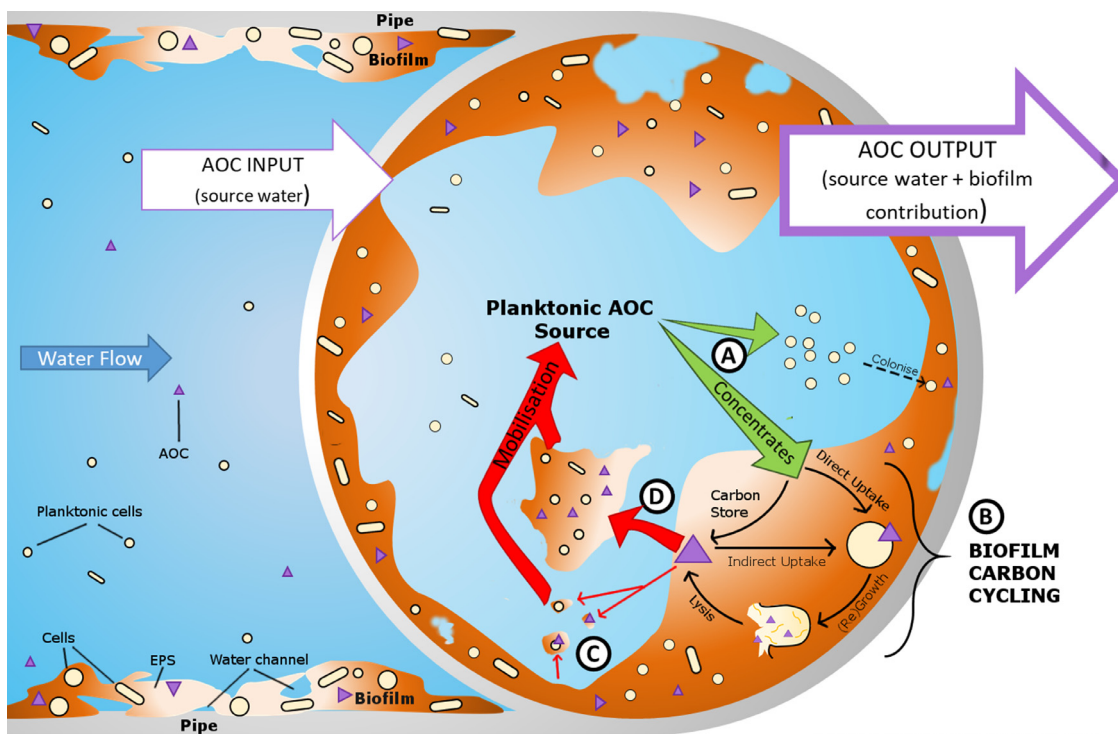
Fig. 7. Conceptual model of assimilable organic carbon (AOC) cycling within DWDS. A) Energy source/supply; B) Cycling of AOC within the biofilm, as an energy source and store; C) Daily mobilisation; D) Event induced mobilisation.

of inorganics, and thus presenting a greater discolouration potential.

During the flushing phase, biofilm samples within all three pipe loop samples exhibited a reduction of cells (both total and intact), confirming that cells were being mobilised into the bulk water. The observed trends in TCC/ICC reduction from biofilm samples between sites were the same as the relationships observed between sites for the turbidity and metals data; the largest TCC/ICC response occurred within Pipe Loop A containing highest AOC concentration within the bulk water. This suggests that mobilisation of a greater concentration of microbial cells could cause an increased discolouration response. However, the greatest proportional change in planktonic TCC or ICC occurred during flushing within Pipe Loop C (the site with the lowest AOC concentration). Therefore, the complex patterns presented herein demonstrate that there is no simple, linear relationship between the amount of cell mobilisation and the discolouration response, and that holistic biofilm analysis is required.

5.3. Conceptual model

AOC release from the biofilm was examined herein for the first time and unexpectedly demonstrated that the rate of AOC release from the biofilm during flushing was the same across field sites, independent of the AOC concentration within the bulk water. All other measured drinking water parameters, including TOC, exhibited a site specific effect during flushing. These results suggest that complex cycling of AOC occurs in the biofilm, in which excess AOC is potentially stored within the biofilm at times of elevated AOC concentration in the bulk water. Carbon and nutrients (e.g. ammonium, nitrates, phosphates) follow a gradient towards the pipe wall, driven by the turbulence of the water. As the biofilm EPS matrix is often negatively charged a number of nutrients will concentrate at the biofilm surface and water channels can facilitate the mass transfer of nutrients/carbon to microorganisms within the biofilm (de Beer and Stoodley, 1995;de Beer et al. 1996). Trace substrates become trapped in the EPS and are only mobilised during small background events or when the shear stress acting upon the biofilm exceeds the internal cohesive strength of the EPS.

A conceptual model is presented in Fig. 7, illustrating the complex cycling of AOC in DWDS, based on the interpretations of data obtained in this study. Central is the idea that biofilms interact with the bulk water through daily background exchange and occasional larger mobilisation events occurring after a change in environmental conditions, such as an increase in the hydraulic shear stress. The AOC concentration within the bulk water not only impacts planktonic microbial growth, but can also be used by microorganisms within the biofilm, further contributing to microbial regrowth within the DWDS. The net effect of pipe dominated areas of a DWDS, is an increase in the AOC concentration, as shown by the purple arrows into and out of the cross section of the conceptual diagram (Fig. 7). Pick et al. (2019) observed an increasing AOC concentration within trunk mains, and a decrease in AOC concentration with service reservoirs within DWDS. We theorise that AOC can be stored within the biofilm; a process which is likely limited by ecological processes occurring within the biofilm, providing a ratio of AOC storage. AOC storage and subsequent release from the biofilm is likely a complex function of the physical composition of the biofilm, in which the EPS plays a key role, and the ecological interactions occurring within the biofilm. The current study focuses on the interactions between AOC and microbial cells, further research is required to understand the interaction between additional biofilm characteristics (e.g. architecture, biochemistry and EPS matrices properties) and AOC cycling within DWDS. The comprehensive model provides a greater understanding of AOC cycling within drinking water, essential in the

management and maintenance of biological stability within DWDS environments.

6. Conclusion

This paper presents the first use of full-scale DWDS simulation experimental facilities at the outlet of WTW to study the impact of different AOC concentrations on biofilm and bulk water quality.

- The AOC concentration within bulk water was found to dictate both the rate of biofilm growth, and the discoloration response the biofilms posed when they are mobilised.
- A high AOC concentration ($>$300 µg C/L) in the bulk water resulted in the greatest growth of cells in the biofilm, and the largest discolouration response as observed for turbidity, iron and manganese.
- New evidence of AOC cycling within the biofilm has advanced our understanding of how and why AOC concentration varies within DWDS and the impacts this has on microbial (re)growth.
- The rate of AOC release from the biofilm into the water column was found to be independent from bulk water AOC concentration. This suggests the need to consider how AOC is used or incorporated into the biofilm.
- A unifying conceptual model is presented that describes the complex AOC processes in DWDS, capturing both bulk water and, previously overlooked, biofilm processes.
- This study found no universal AOC threshold for biological stability, due to the interaction and influence of both planktonic and biofilm process.

Ultimately, the information gained in this study will enable better management of DWDS environments to maintain the quality of drinking water from source to tap.

Declaration of Competing Interest

None.

Supplementary materials

Supplementary material associated with this article can be found, in the online version, at doi:10.1016/j.watres.2021.117147.

References

Aggarwal, S., Jeon, Y., Hozalski, R.M., 2015. Feasibility of using a particle counter or flow-cytometer for bacterial enumeration in the assimilable organic carbon (AOC) analysis method. Biodegradation 1–11.

Characklis, W.G., 1988. *Bacterial (re)growth in Distribution systems,* Project Report. American Water Works Association, USA.

De Beer, D., Stoodley, P., 1995. Relation between the structure of an aerobic biofilm and transport phenomena. Water Science and Technology 32 (8), 11–18.

De Beer, D., Stoodley, P., Lewandowski, Z., 1996. Liquid flow and mass transport in heterogeneous biofilms. Water Res. 30 (11), 2761–2765.

Deines, P., Sekar, R., Husband, P.S., Boxall, J.B., Osborn, A.M., Biggs, C.A., 2010. A new coupon design for simultaneous analysis of in situ microbial biofilm formation and community structure in drinking water distribution systems. Appl. Microbiol. Biotechnol. 87 (2), 749–756.

Douterelo, I., Sharpe, R., Boxall, J., 2014. Bacterial community dynamics during the early stages of biofilm formation in a chlorinated experimental drinking water distribution system: implications for drinking water discolouration. J. Appl. Microbiol. 117 (1), 286–301.

Douterelo, I., Jackson, M., Solomon, C., Boxall, J., 2016. Microbial analysis of in situ biofilm formation in drinking water distribution systems: implications for monitoring and control of drinking water quality. Appl. Microbiol. Biotechnol. 100 (7), 3301–3311.

Douterelo, I., Fish, K.E., Boxall, J.B., 2018. Succession of bacterial and fungal communities within biofilms of a chlorinated drinking water distribution system. Water Res. 141, 74–85.

Dunne, W.M., 2002. Bacterial adhesion: seen any good biofilms lately? Clin. Microbiol. Rev. 15 (2), 155–166.

Drinking Water Inspectorate (DWI), 2017. What Are the Drinking Water Standards?. Drinking Water Inspectorate, London Technical report.

Escobar, I.C., Randall, A.A., Taylor, J.S., 2001. Bacterial growth in distribution systems: effect of assimilable organic carbon and biodegradable dissolved organic carbon. Environ. Sci. Tech.35 (17) 3442–3447.

Karthikeyan, S., Korber, D.R., Wolfaardt, G.M., Caldwell, D.E., 2001. Adaptation of bacterial communities to environmental transitions from labile to refractory substrates. Int. Microbiol. 4 (2), 73–80.

Fish, K.E., 2013. The Impact of Hydraulic Regime Upon Biofilms in Drinking Water Distribution Systems PhD Thesis. University of Sheffield.

Fish, K., Osborn, A.M., Boxall, J.B., 2017. Biofilm structures (EPS and bacterial communities) in drinking water distribution systems are conditioned by hydraulics and influence discolouration. Sci. Total Environ. 593, 571–580.

Fish, K.E., Reeves-McLaren, N., Husband, S., Boxall, J., 2020. Unchartered waters: the unintended impacts of residual chlorine on water quality and biofilms. NPJ Biofilms Microbiomes 6 (1), 1–12.

Gillespie, S., Lipphaus, P., Green, J., Parsons, S., Weir, P., Juskowiak, K., Jefferson, B., Jarvis, P., Nocker, A., 2014. Assessing microbiological water quality in drinking water distribution systems with disinfectant residual using flow cytometry. Water Res. 65, 224–234.

Husband, S., Boxall, J.B., 2010. Field studies of discoloration in water distribution systems: model verification and practical implications. J. Environ. Eng.136 (1) 86–94.

Husband, P.S., Boxall, J.B., Saul, A.J., 2008. Laboratory studies investigating the processes leading to discolouration in water distribution networks. Water Res. 42 (16), 4309–4318.

Husband, S., Fish, K.E., Douterelo, I., Boxall, J., 2016. Linking discolouration modelling and biofilm behaviour within drinking water distribution systems. Water Sci. Tech. 16 (4), 942–950.

LeChevallier, M.W., Shaw, N.E., Kaplan, L.A., Bott, T.L., 1993. Development of a rapid assimilable organic carbon method for water. Appl. Environ. Microbiol. 59 (5), 1526–1531.

LeChevallier, M.W., Welch, N.J., Smith, D.B., 1996. Full-scale studies of factors related to coliform (re)growth in drinking water. Appl. Environ. Microbiol. 62 (7), 2201–2211.

LeChevallier, M.W., Schneider, O.D., Weinrich, L.A., Jjemba, P.K., Evans, P.J., Hooper, J.L., Chappell, R.W., 2015. An Operational Definition of Biostability in Drinking Water. Water Research Foundation, Denver.

Liu, W., Wu, H., Wang, Z., Ong, S.L., Hu, J.Y., Ng, W.J., 2002. Investigation of assimilable organic carbon (AOC) and bacterial (re)growth in drinking water distribution system. Water Res. 36 (4), 891–898.

Nescerecka, A., Rubulis, J., Vital, M., Juhna, T., Hammes, F., 2014. Biological instability in a chlorinated drinking water distribution network. PLoS ONE 9 (5), e96354.

Ohkouchi, Y., Ly, B.T., Ishikawa, S., Kawano, Y., Itoh, S., 2013. Determination of an acceptable assimilable organic carbon (AOC) level for biological stability in water distribution systems with minimized chlorine residual. Environ. Monit. Assess. 185 (2), 1427–1436.

Okabe, S., Kokazi, T., Watanabe, Y., 2002. Biofilm formation potentials in drinking waters treated by different advanced treatment processes. Water Sci. Tech. 2 (4), 97–104.

Okabe, S., Kindaichi, T., Ito, T., Satoh, H., 2004. Analysis of size distribution and areal cell density of ammonia-oxidizing bacterial microcolonies in relation to substrate microprofiles in biofilms. Biotechnol. Bioeng. 85 (1), 86–95.

Picioreanu, C., Van Loosdrecht, M.C., Heijnen, J.J., 2001. Two-dimensional model of biofilm detachment caused by internal stress from liquid flow. Biotechnol. Bioeng. 72 (2), 205–218.

Pick, F.C., Fish, K.E., Biggs, C.A., Moses, J.P., Moore, G., Boxall, J.B., 2019. Application of enhanced assimilable organic carbon method across operational drinking water systems. PLoS ONE (12) 14.

R Foundation for Statistical Computing Platform, (2018). The R Project for Statistical Computing. Available online: https://www.r-project.org/ (accessed January 2018).

Ramseier, M.K., Peter, A., Traber, J., von Gunten, U., 2011. Formation of assimilable organic carbon during oxidation of natural waters with ozone, chlorine dioxide, chlorine, permanganate, and ferrate. Water Res. 45 (5), 2002–2010.

Sharp, R.R., Camper, A.K., Crippen, J.J., Schneider, O.D., Leggiero, S., 2001. Evaluation of drinking water biostability using biofilm methods. J. Environ. Eng.127 (5) 403–410.

Sharpe, R.L., Biggs, C.A., Boxall, J.B., 2017. Hydraulic conditioning to manage potable water discolouration, pp. 1–11.

Stoodley, P., Hall-Stoodley, L., &Lappin-Scott, H.M. (2001). Growth Biofilms Pt B, vol. 337, pp. 306–318.

Van der Kooij, D., 1992. Assimilable organic carbon as an indicator of bacterial (re)growth. American Water Works Association 57–65.

Van der Kooij, D., 2003. Managing (re)growth in Drinking Water Distribution systems. Heterotrophic plate Counts and Drinking-Water Safety. IWA Publishing, London, United Kingdom.

Van der Kooij, D., Visser, A., Hijnen, W., 1982. Determining the concentration of easily assimilable organic carbon in drinking water. American Water Works Association 74 (10), 540–543.

Van der Kooij, D., Veenendaal, H.R., Baars-Lorist, C., van der Klift, D.W., Drost, Y.C., 1995. Biofilm formation on surfaces of glass and teflon exposed to treated water. Water Res. 29 (7), 1655–1662.

Volk, C.J., LeChevallier, M.W., 1999. Impacts of the reduction of nutrient levels on bacterial water quality in distribution systems. Appl. Environ. Microbiol. 65 (11), 4957–4966.

Wang, Q., Tao, T., Xin, K., 2014. The Relationship between Water Biostability and Initial Bacterial Growth Variations to Different Organic Carbon Concentrations. Procedia Eng. 89, 160–167.